PNNL-24073

Pacific Northwest
NATIONAL LABORATORY
Proudly Operated by Battelle Since 1965

Fuel Thermo-physical Characterization Project: Evaluation of Models to Calculate Thermal Diffusivity of Layered Composites

February 2015

DE Burkes
AJ Casella
LD Gardner
AM Casella
TK Huber*
H Breitkreutz*

* Technische Universität München

U.S. DEPARTMENT OF ENERGY

Prepared for the U.S. Department of Energy
under Contract DE-AC05-76RL01830

PACIFIC NORTHWEST NATIONAL LABORATORY
operated by
BATTELLE
for the
UNITED STATES DEPARTMENT OF ENERGY
under Contract DE-AC05-76RL01830

Printed in the United States of America

Available to DOE and DOE contractors from the
Office of Scientific and Technical Information,
P.O. Box 62, Oak Ridge, TN 37831-0062;
ph: (865) 576-8401
fax: (865) 576-5728
email: reports@adonis.osti.gov

Available to the public from the National Technical Information Service
5301 Shawnee Rd., Alexandria, VA 22312
ph: (800) 553-NTIS (6847)
email: orders@ntis.gov <http://www.ntis.gov/about/form.aspx>
Online ordering: http://www.ntis.gov


This document was printed on recycled paper.
(8/2010)

PNNL-24073

Fuel Thermo-physical Characterization Project: Evaluation of Models to Calculate Thermal Diffusivity of Layered Composites

DE Burkes
AJ Casella
LD Gardner
AM Casella
TK Huber*
H Breitkreutz*

* Technische Universität München

February 2015

Prepared for
the U.S. Department of Energy
under Contract DE-AC05-76RL01830

Pacific Northwest National Laboratory
Richland, Washington 99352

Summary

The Office of Material Management and Minimization Fuel Thermo-physical Characterization Project at Pacific Northwest National Laboratory (PNNL) is tasked with using PNNL facilities and processes to receive irradiated low enriched uranium-molybdenum fuel plate samples and perform analyses in support of the Office of Material Management and Minimization Reactor Conversion Program. This work is in support of the Fuel Development Pillar that is managed by Idaho National Laboratory. A key portion of the scope associated with this project was to measure the thermal properties of fuel segments harvested from plates that were irradiated in the Advanced Test Reactor. Thermal diffusivity of samples prepared from the fuel segments was measured using laser flash analysis. Two models, one developed by PNNL and the other developed by the Technische Universität München (TUM), were evaluated to extract the thermal diffusivity of the uranium-molybdenum alloy from measurements made on the irradiated, layered composites. The experimental data of the "TC" irradiated fuel segment was evaluated using both models considering a three-layer and five-layer system. Both models are in acceptable agreement with one another and indicate that the zirconium diffusion barrier has a minimal impact on the overall thermal diffusivity of the monolithic U-Mo fuel.

Acknowledgments

The authors wish to acknowledge Mr. Jason Schulthess, Dr. Barry Rabin, and Dr. Mitchell Meyer from Idaho National Laboratory for the support of this work. The authors wish to acknowledge those at Pacific Northwest National Laboratory who were involved in the preparation of samples and performance of measurements. The authors wish to acknowledge Sharon Eaton for her assistance with formatting and copyediting and Dr. David Senor for his peer review of this report. Finally, the authors wish to acknowledge the sponsor, the Global Threat Reduction Initiative (NA-21), for the opportunity to conduct this work under contract DE-AC05-76RL01830.

Acronyms and Abbreviations

AA	aluminum alloy
AFIP	Advanced Test Reactor Full-size Plate In Center Flux Trap Position
HEU	high-enriched uranium
LFA	laser flash analysis
PNNL	Pacific Northwest National Laboratory
TUM	Technische Universität München
U-Mo	uranium-molybdenum alloy

Contents

Figures

Tables

1.0 Introduction

The uranium-molybdenum (U-Mo) alloy is currently under development as a potential fuel design that will allow high-performance research reactors to convert to low-enriched uranium in lieu of operation with high-enriched uranium (HEU), the latter being a concern for potential diversion and use in crude nuclear weapons. The Office of Material Management and Minimization Reactor Conversion Program and partners worldwide have embarked on a mission to develop and qualify the U-Mo alloy for use in some of the world's most powerful research and test reactors currently operating with HEU. The evolution of the thermal conductivity during irradiation of research and test reactor fuel plays a significant role in fuel element performance. It is important to investigate the change in thermal conductivity as a function of fission density and/or ^{235}U burnup, as well as temperature, in order to correctly simulate the heat fluxes and temperatures in the fuel meat[1] during both normal reactor operation and potential accident scenarios. Accordingly, such data are needed during the evaluation and qualification process of this new fuel type. In addition, the thermal conductivity of spent fuel might include information needed to identify and assess mechanisms that potentially lead to the accelerated failure mechanisms, e.g., swelling.

Thermal conductivity is typically not measured directly; rather it is a function of the material's density, thermal diffusivity, and specific heat. Each of these properties can be measured separately. A change in the fuel density is driven mainly by fission products (both gaseous and solid) that agglomerate in the fuel meat during irradiation. This property can be measured by immersion, characterizing changes in fuel plate dimension, or pycnometry. Specific heat capacity of the fuel can change as a result of the change in the material composition, as the ^{235}U is consumed leading to a build-up of various fission and neutron capture products. The specific heat capacity can be obtained with a Differential Scanning Calorimeter. The final property, thermal diffusivity, can also be affected by changes in material composition, formation of intermetallics as a result of irradiation (i.e., irradiation enhanced diffusion), build-up of porosity as a result of gaseous fission products, or other material issues such as cracking in the fuel. The thermal diffusivity is most commonly obtained with a Laser Flash Apparatus (LFA). The Pacific Northwest National Laboratory (PNNL) has installed a suite of thermal analysis instruments in hot cells for the examination of irradiated reactor fuel. This set-up provides a unique environment to investigate all three properties (density, thermal diffusivity, and specific heat capacity) that are necessary for the calculation of the thermal conductivity of irradiated U-Mo fuels. Additionally, an optical microscope has been installed in a hot cell to quantify the structural changes in the fuel, which lead to a change in the thermal properties.

Plate-type fuel, such as that used in research and test reactors, presents a unique challenge to extraction of fuel meat properties based on composite measurements. The fuel meat is clad by a high-conductivity material, typically aluminum alloy 6061 (AA6061), and can also contain intermediate layers to inhibit interaction between the fuel and cladding during fabrication and/or irradiation. Thus, the fuel can be represented by a composite consisting of three or more layers. It should be pointed out that chemical or mechanical extraction of the fuel meat from the composite for testing independently from the clad and barrier layers would be challenging and impractical. Furthermore, this would be an undesirable approach since the integrated behavior of the composite system would be lost, and features such as uniformity and contact resistance inherent to a composite system would be lost. Thus, extraction of fuel meat properties, such as thermal diffusivity, from multi-layered composites requires the use of numerical

[1] "Fuel meat" is defined here as a solid piece of fuel material, also referred to as "monolithic" fuel.

methods. Two such methods have been developed for the LFA method to measure the thermal diffusivity of layered composites, i.e., plate-type fuel, and are discussed in this report.

2.0 Description of the Models

This section provides a brief description on the theory and operation of both models. For simplicity, the model developed at PNNL is referred to as the "PNNL model," while the model developed at Technische Universität München (TUM) is referred to as the "TUM model."

2.1 PNNL Model Description

A simple model developed from the mathematical analysis of the flash method for measuring the thermal diffusivity of layered composites was adapted to extract the thermal diffusivity of the fuel meat as a function of temperature (Lee 1975). The model is based on a three-layer system and assumes 1) one-dimensional heat flow, 2) no heat loss from the sample surfaces, 3) no interfacial thermal contact resistance, 4) each layer is homogeneous, 5) heat pulse is uniformly absorbed on the front surface, and 6) only one thermophysical property is unknown in one of the layers (in this case, thermal diffusivity). The heat diffusion equation is described mathematically for each layer in Equation 1.

$$\frac{\partial^2\theta_j(z,t)}{\partial z^2} = \frac{1}{\alpha_j}\frac{\partial\theta_j(z,t)}{\partial t} \text{ for j = 1, 2, 3} \quad (1)$$

The boundary conditions for the heat diffusion equation are represented in Equations 2a-f, and the initial condition is represented in Equation 3.

$$-k_1\frac{\partial\theta_1(z_1,t)}{\partial z} = w(t) \quad (2a)$$

$$\theta_1(0,t) = \theta_2(0,t) \quad (2b)$$

$$k_1\frac{\partial\theta_1(0,t)}{\partial z} = k_2\frac{\partial\theta_2(0,t)}{\partial z} \quad (2c)$$

$$\theta_2(z_2,t) = \theta_3(z_2,t) \quad (2d)$$

$$k_2\frac{\partial\theta_2(z_2,t)}{\partial z} = k_3\frac{\partial\theta_3(z_2,t)}{\partial z} \quad (2e)$$

$$k_3\frac{\partial\theta_3(z_3,t)}{\partial z} = 0 \quad (2f)$$

$$\theta_1(z,0) = \theta_2(z,0) = \theta_3(z,0) = 0 \quad (3)$$

In Equations 2 and 3, α_j is the thermal diffusivity of the *jth* layer, θ_j is the temperature of the *jth* layer, and z is defined by Equation 4a-c where l is the thickness of the *jth* layer.

$$z_1 = -l_1 \quad (4a)$$

$$z_2 = l_2 \quad (4b)$$

$$z_3 = l_2 + l_3 \quad (4c)$$

Following the derivation of Lee (Lee 1975), the simplified equation of the normalized temperature rise on the back face following a heat pulse to the front face is represented by Equations 5-14:

$$V = 1 + 2\sum_{k=1}^{\infty} \frac{(\omega_1 X_1+\omega_2 X_2+\omega_3 X_3+\omega_4 X_4) Q(\gamma_k,\eta_3,t)}{\omega_1 X_1 \cos(\omega_1\gamma_k)+\omega_2 X_2 \cos(\omega_2\gamma_k)+\omega_3 X_3 \cos(\omega_3\gamma_k)+\omega_4 X_4 \cos(\omega_4\gamma_k)} \quad (5)$$

where

$$X_1 = H_{1/3}\eta_{3/1} + H_{1/2}\eta_{2/1} + H_{2/3}\eta_{3/2} + 1 \quad (6)$$

$$X_2 = H_{1/3}\eta_{3/1} - H_{1/2}\eta_{2/1} + H_{2/3}\eta_{3/2} - 1 \quad (7)$$

$$X_3 = H_{1/3}\eta_{3/1} - H_{1/2}\eta_{2/1} - H_{2/3}\eta_{3/2} + 1 \quad (8)$$

$$X_4 = H_{1/3}\eta_{3/1} + H_{1/2}\eta_{2/1} - H_{2/3}\eta_{3/2} - 1 \quad (9)$$

$$\omega_1 = \eta_{1/3} + \eta_{2/3} + 1 \quad (10)$$

$$\omega_2 = \eta_{1/3} + \eta_{2/3} - 1 \quad (11)$$

$$\omega_3 = \eta_{1/3} - \eta_{2/3} + 1 \quad (12)$$

$$\omega_4 = \eta_{1/3} - \eta_{2/3} - 1 \quad (13)$$

$$Q(\gamma,\eta,t) = \int_0^t h(\mathcal{E}) exp\left(\frac{-\gamma^2(t-\mathcal{E})}{\eta^2}\right) d\mathcal{E} \quad (14)$$

An instantaneous heat pulse produced by the laser was assumed for the term $Q(\gamma,\eta,t)$. The $h(\varepsilon)$ is a normalized heat pulse function and the ε is the fictitious variable for the integration. The γ_k is the *kth* positive root of the characteristic equation represented in Equation 15.

$$U(\gamma) = X_1 \sin(\omega_1\gamma) + X_2 \sin(\omega_2\gamma) + X_3 \sin(\omega_3\gamma) + X_4 \sin(\omega_4\gamma) = 0 \quad (15)$$

The relative volumetric heat capacity $H_{i/j}$ and the square root of relative heat diffusion time are defined by Equations 16 and 17.

$$H_{i/j} = \frac{H_i}{H_j} \quad (16)$$

$$\eta_{i/j} = \frac{\eta_i}{\eta_j} \quad (17)$$

The volumetric heat capacity H_j and the square root of heat diffusion time η_j of the *jth* layer are defined by Equations 18 and 19, where a is the cross-sectional area of the sample, ρ_j is the density, and c_j is the specific heat capacity of the *jth* layer.

$$H_j = a\rho_j c_j l_j \quad (18)$$

$$\eta_j = \sqrt{\left(\frac{l_j^2}{\alpha_j}\right)} \tag{19}$$

The model was reproduced in Wolfram Mathematica v. 8.0.0.0 for execution. The composite thermal diffusivity of the fuel plate was used as an input to the model. The half rise time of the composite was determined using Parker's method (Parker et al. 1961) represented by Equation 20.

$$\alpha = \frac{0.139 l^2}{t_{1/2}} \tag{20}$$

The PNNL model iterates upon the half rise time of the composite to determine the half rise time of the unknown layer. Once the unknown layer half rise time is determined, Equation 20 is then used to calculate the thermal diffusivity of the unknown layer. The remaining model inputs were calculated using the experimental data obtained for density, specific heat capacity, and the layer thicknesses that were obtained from optical microscopy. For the three-layer calculations, the model inputs were calculated assuming Zr as part of the fuel layer. In other words, the three layers were 1) the bottom AA6061 cladding layer, 2) the composite fuel + zirconium layer, and 3) the top AA6061 cladding layer. The properties of the AA6061 were fully described based upon literature values, while the heat capacity and density values of the combined fuel + zirconium layer were determined by Neumann-Kopp and rule of mixtures using experimental measurements (described in Section 3.0). The model output was the thermal diffusivity value for the composite fuel + zirconium combined layer. The PNNL five-layer calculation is actually a nested three-layer model. First, the-three layer model was employed as just described. Then, a second three-layer model calculation was executed. In the second calculation, the three layers were the bottom zirconium layer, the fuel layer, and the top zirconium layer. The combined fuel + zirconium output thermal diffusivity determined from the first three-layer calculation was used as the input composite thermal diffusivity value for the second three-layer calculation, while the properties of the Zr were fully described based upon literature values. Again, the heat capacity and density values of the fuel itself were determined by Neumann-Kopp and rule of mixtures using experimental measurements (described in Section 3.0). The result of the second three-layer calculation was therefore the thermal diffusivity of the fuel itself.

2.2 TUM Model Description

ThermoFit ML is a program to evaluate the thermal diffusivity from LFA measurements of samples composed of one or multiple layers. Solutions of the 1D heat conduction equation including laser pulse corrections and heat losses are used to determine the thermal diffusivity of the specimen. For analyzing a multiple layer sample, only the thermal diffusivity of one layer may be unknown, or the result will most likely not be unique, i.e., the sensitivity to small uncertainties is too large to allow for an adequate determination of the thermal diffusivities. Furthermore, the program requires the thickness of each layer as well as the thermal diffusivity, the density and specific heat, or alternatively the thermal conductivity of each additional material as input parameters for the simulation. In contrast to the PNNL model, this model calculates the thermal diffusivity of the layer of interest directly from the raw data temperature curve of the composite, while the PNNL model uses the thermal diffusivity value of the composite material, which is already calculated via a one-layer model. The model is implemented in a .NET library that is visualized through the ThermoProp-Software.

In the first step, the lower and the upper baselines are determined from the data to calculate the minimum and maximum voltage differences in the thermal signal (T_0 and T_{max}) at the sample backside. An example of a typical time-temperature profile obtained from an LFA measurement is provided in Figure 2.1.

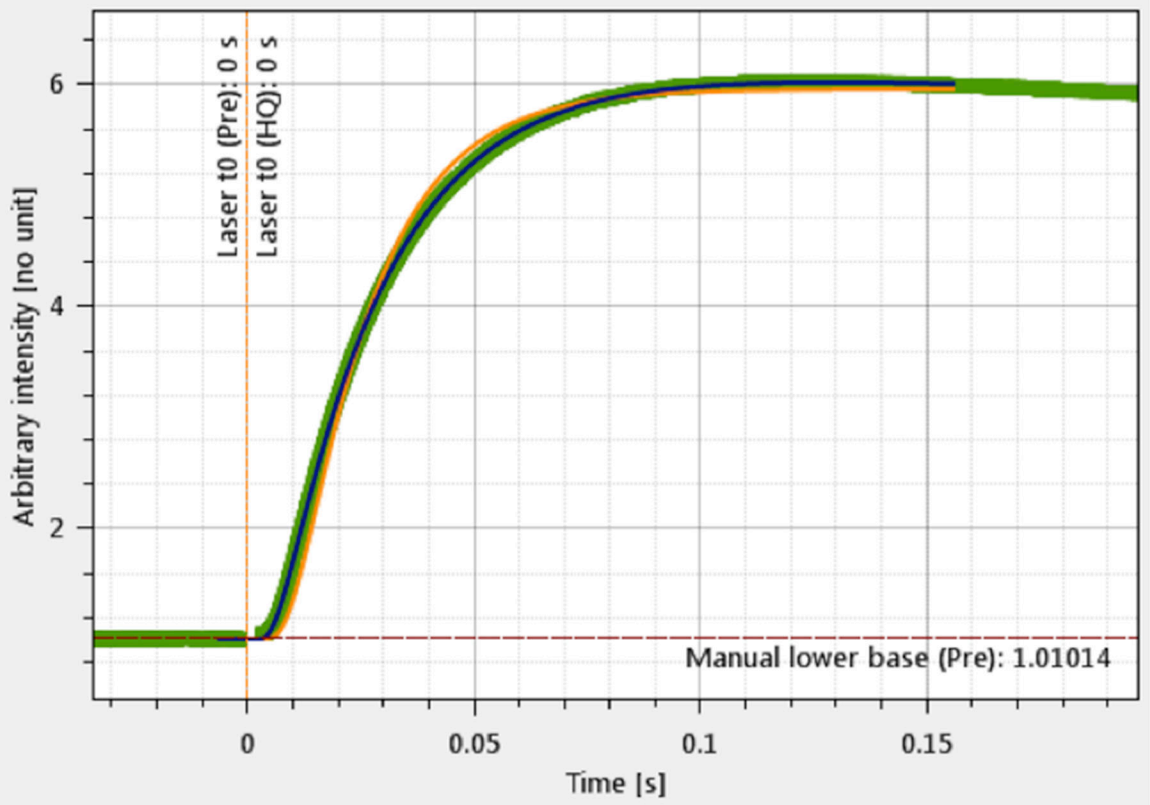

Figure 2.1. Example of a Typical Time-Temperature Profile (Green Data Points) Obtained from an LFA Measurement. The red dashed line shows the lower baseline, i.e., the minimum temperature. The orange line is the result of a one-layer fit that provides start values

The backside temperature curve for an isolated one-layer system can be approached by the analytical solution of the heat diffusion equation (Parker et al. 1961), shown in Equation 21. It is used in the PNNL model to obtain the start value for the thermal diffusivity of the composite. In the TUM model, the results are used as start values for the numerical simulation, which takes additional properties into account.

$$T_{norm}(L,t) = \frac{T(L,t) - T_0}{T_{max} - T_0} = 1 + 2 * \sum_{n=1}^{\infty} (-1)^n * exp\left(-n^2 \frac{\pi\alpha(t - t_0)}{L^2}\right) \quad (21)$$

In Equation 21, $T_{norm}(L,t)$ is the normalized temperature derived from the ratio between the actual backside temperature $T(L,t)$ at time t and position L, where L is the thickness of the sample, and the maximum temperature T_{max}. As only the temperature interval is relevant, the baseline temperature T_0 is subtracted from $T(L,t)$ and T_{max}.

The sum has to be cut off after some term to allow for numerical calculation of the solution of Equation 21. However, in this case for $t \leq t_0$, the function for the normalized temperature does not yield

$T_{norm}(t_0)$ but rather approaches negative infinity at t_0 with a sharp bend. Taking more terms into account, the sharp bend moves closer to t_0 and away from the relevant data points. Twenty-five terms are usually a good choice to sum over; more terms take longer computing time but do not significantly improve the result. For a very large number of terms, the solution may become numerically unstable due to the exponential factor in the sum. To avoid this, the actual implementation does not allow for $T_{norm}(L,t) < 0$, i.e. $T_{norm,impl.}(L,t) = \max\big(0, T_{norm}(L,t)\big)$.

This solution is only for single layers and does not take into account the time-dependent intensity of the laser flash and heat losses. However, it is sufficient to calculate the initial values for the simulation-based fit, i.e., the average thermal diffusivity of the whole sample and the time of the laser shot t_0. As the t_0 parameter and the thermal diffusivity are strongly linked in the correlation matrix, it is greatly advantageous to specify it manually if it is known in advance—often, $t_0 = 0$.

This analytical pre-solution is then improved by the numerical solution of the 1D heat diffusion equation with explicit Euler, represented by Equation 22.

$$T_n^{k+1} = T_n^k + \frac{\alpha \Delta t}{\Delta x_i^2}\left(T_{n+1}^k - 2T_n^k + T_{n-1}^k\right) \tag{22}$$

In Equation 22, Δx_i is the special discretization in layer i, which may be different from layer to layer. $\Delta t = (k+1) - k$ is the time discretization.

Boundary conditions used for the TUM model are represented by Equations 23a-f and described in this section. Incoming heat flux from the laser pulse hits the sample on the front side with convective and radiative cooling

$$T_{0,0}^{k+1} = T_{0,0}^k + \frac{2\alpha_0 \Delta t}{\Delta x_0^2}\Big[\Big(T_{0,1}^k - T_{0,0}^k + \underbrace{\Delta x_0 S_0(k)}_{\text{laser}}\Big) + \underbrace{a_1\left(T_{0,0}^k - T_{0,0}^0\right)}_{\text{convective}} + \underbrace{a_4\left(T_{0,0}^k - T_{0,0}^0\right)^4}_{\text{radiative}}\Big] \tag{23a}$$

with $S_0(t)$ as the normalized laser signal:

$$S_0(k) = \frac{\Delta T_{norm}}{\lambda_0} \cdot \frac{\int_k^{k+1} Laser(t)\, dt}{\int_0^{\infty} Laser(t) dt} \cdot \sum_i \frac{\lambda_i}{\alpha_i} d_i \tag{23b}$$

For the unknown layer, the thermal conductivity, λ, is calculated from the trial solution for the thermal diffusivity α and the known density ρ and specific heat capacity C_p.

$$\Delta T_{norm} = T_{max} - T_0 \tag{23c}$$

Continuous boundary conditions at the layer interfaces, for heat flux and for temperature, are used according to Equations 23d and 23e.

$$T_{A,N}^{k+1} = T_{A,N}^k + \frac{2\alpha_A \alpha_B \Delta t}{(\alpha_B \lambda_A \Delta x_A + \alpha_A \lambda_B \Delta x_B)}\left(\frac{\lambda_B}{\Delta x_B}\left(T_{B,1}^k - T_{B,0}^k\right) - \frac{\lambda_A}{\Delta x_A}\left(T_{A,N}^k - T_{A,N-1}^k\right)\right) \tag{23d}$$

$$T_{B,0}^{k+1} = T_{A,N}^{k+1} \tag{23e}$$

Cooling conditions at the back of the sample and at the front side (except for the laser pulse) are described by Equation 23f.

$$T_{M,N}^{k+1} = T_{M,N}^{k} + \frac{2\alpha_M \Delta t}{\Delta x_M^2}\left[\left(-T_{M,N}^{k} + T_{M,N-1}^{k}\right) + a_1\left(T_{M,N}^{k} - T_{M,N}^{0}\right) + a_4\left(T_{M,N}^{k} - T_{M,N}^{0}\right)^4\right] \quad (23f)$$

In Equations 23a-f, N_i is the number of special discretization steps and λ_i is the thermal conductivity of the layer i. M is the outermost layer index and a_1 and a_4 are cooling factors that are assumed to be temperature independent and equal for both sides of the sample. Note that due to the cooling correction, the actual curve does not necessarily read $T = T_{max}$, which would correspond to the upper baseline in the Parker model. In the simulation, T_{max} serves as a free parameter for the normalization. Other fixed parameters are T_0, t_0, T_{max}, a_1, a_4 and α_x. All of these parameters, except α_x, can optionally be fixed manually. It is recommended to fix especially T_0 and t_0 for higher accuracy.

The initial condition at t_0 is described by Equation 24.

$$T_{i,n}^{0} = T_0 \quad (24)$$

The result of the simulation $T_{M,N}$ is the temperature curve at the rear side of the sample that is actually measured in the experiment. An adapted version of the Levenberg-Marquardt algorithm (Marquardt 1963) is used to solve the inherent optimization problem by comparing the numerical solution from the differential equation to the actual data curve. In other words, the heat conduction equation is solved with continuously adapted parameters until the squared distance χ^2 between the measured data and the solution from the simulation is minimal.

The same inputs have been used for the data evaluation as in the PNNL model. First, the three-layer system—consisting of cladding, Zr interlayer plus fuel meat and again, cladding material—was analyzed. Afterwards, the model was conducted as five-layer system, counting the Zr interlayer as separate layer.

3.0 Experimental Measurements

This section describes the calculation of data used as input into the two models. The data used to evaluate the two models was obtained from Segment "TC" that was harvested from the Advanced Test Reactor Full-size Plate in Center Flux Trap Position (AFIP)-2BZ (containing a Zr diffusion barrier). The experimental methods and materials used to obtain the experimental measurements of Segment "TC" have been reported previously (Burkes et al. 2013).

3.1 Layer Thicknesses

Because both models consider only one unknown property (e.g., thermal diffusivity), it is necessary to provide the thickness, the specific heat capacity, and the density of each layer of the composite measured. The individual layer thicknesses used in the models were determined using optical microscopy measurements and are summarized in Table 3.1. Data presented in the table are the average and standard deviations obtained from two samples. Note that for the three-layer model evaluations, the thickness of the Zr layer was added to the thickness of the U-10Mo layer.

Table 3.1. Summary of Individual Layer Thicknesses Determined Using Optical Microscopy

Layer	Overall Thickness, μm
AA6061 (upper)	443 ± 20.6
Zirconium (upper)	31.5 ± 7.02
U-10Mo	391 ± 15.6
Zirconium (lower)	34.7 ± 8.75
AA6061 (lower)	445 ± 46.4
Total Plate	1335 ± 39.1

3.2 Density

Temperature-dependent density of the aluminum alloy 6061 (AA6061) cladding and Zr diffusion barrier were determined using the correlations of Mills (Mills 2002) and Fink and Leibowitz (Fink and Leibowitz 1995), respectively. The density of these components was assumed to be unaffected by irradiation. Pycnometry measurements performed on both the TC-LFA1 and TC-LFA2 samples were used to determine the average composite density at room temperature. The average and standard deviation of the sample measurements are summarized in Table 3.2. The volume fraction of each layer was determined using the OM thicknesses provided in Table 3.1. Assuming that Zr is part of the U-Mo (for a three-layer system), the result is a volume fraction of 66% AA6061 and 34% Zr + U-Mo. The density of the Zr + U-Mo layer was determined using the room temperature composite density measurements and the rule of mixtures. The density of the U-Mo layer (for a five-layer system) was determined using the same method and volume fractions of 66% AA6061, 5% Zr, and 29% U-Mo. Note that the average density of the fuel layer provided in Table 3.2 was used as the input into the model depending on whether a three-layer or five-layer case was being considered along with the temperature-dependent densities of the remaining layers (e.g., AA6061 and/or Zr).

Table 3.2. Average Room Temperature Density of the TC-LFA1 and TC-LFA2 Samples

	Density, g•cm^{-3}
Composite	6.14 ± 0.036
Zr + U-Mo (3-layer)	12.8 ± 0.106
U-Mo (5-layer)	13.9 ± 0.124

3.3 Specific Heat Capacity

Temperature-dependent specific heat capacity of the AA6061 cladding and Zr diffusion barrier were determined using the correlations of Mills (Mills 2002) and Fink and Leibowitz (Fink and Leibowitz 1995), respectively. Although there will be minor modifications to the chemical composition of these constituents as a function of irradiation, e.g., transmutation of silicon in the AA6061, the influence of these modifications on specific heat capacity behavior is likely very minor and well within the uncertainty associated with the measurements. Thus, the U-Mo fuel meat ($Cp_{U\text{-}Mo}$) extractions consider that any specific heat capacity change in the measured composite is because of a change in the fuel meat itself. The specific heat capacity of the fuel layer was determined using the composite specific heat capacity measurements and the Neumann-Kopp approximation, where the mass fraction of each layer was determined using the OM thickness provided in Table 3.1 and the temperature-dependent densities of the AA6061 and Zr described in Section 3.2. For the three-layer system, the Zr was assumed to be part of the U-Mo, while for the five-layer system, the specific heat capacity of only the U-Mo was determined. Note that the specific heat capacity of the fuel layer calculated at the temperature that the LFA measurement was conducted was used as the input into each model. The average specific heat capacities of the composite, Zr + U-Mo (three-layer), and U-Mo (five-layer) as a function of temperature are provided in Figure 3.1.

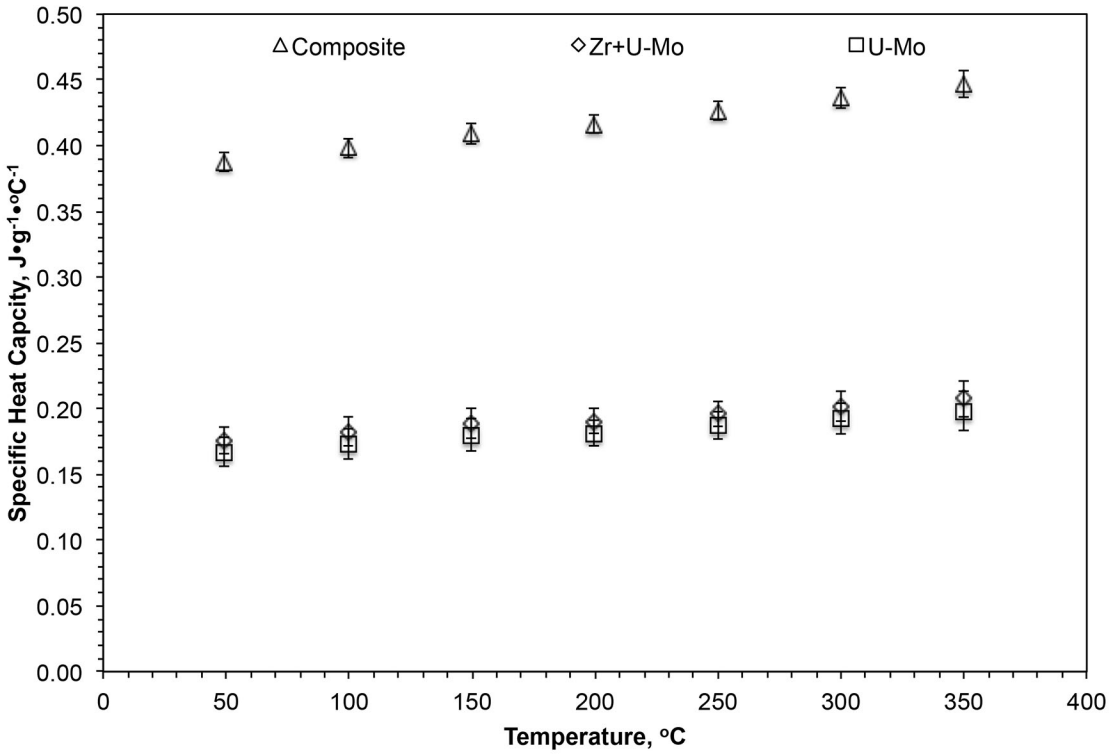

Figure 3.1. Average Specific Heat Capacity of Segment TC as a Function of Temperature for the Composite, Zr + U-Mo, and U-Mo

3.4 Thermal Diffusivity

Temperature-dependent thermal diffusivity of the AA6061 cladding and Zr diffusion barrier was obtained from the temperature-dependent thermal conductivity relations provided in MIL-HDBK-5H (DOD 1998) and Fink and Leibowitz (Fink and Leibowitz 1995), respectively, and the density and specific heat capacity values described in Sections 3.2 and 3.3. NETZSCH Proteus software Version 6.0.0 was used to calculate composite thermal diffusivity using the Cape-Lehman + pulse correction model (Cape and Lehman 1963) that accounts for any heat transfer from the sample to the measurement environment and for finite pulse width effects (given the relative thinness of the samples). LFA measurements conducted on samples TC-LFA1 and TC-LFA2, shown in Figure 3.2 as a function of temperature, were used as the composite thermal diffusivity inputs to the models. Note that the TC-LFA2 sample delaminated at 300 ^{o}C, thus, the significantly lower thermal diffusivity values at 300 ^{o}C and 350 ^{o}C.

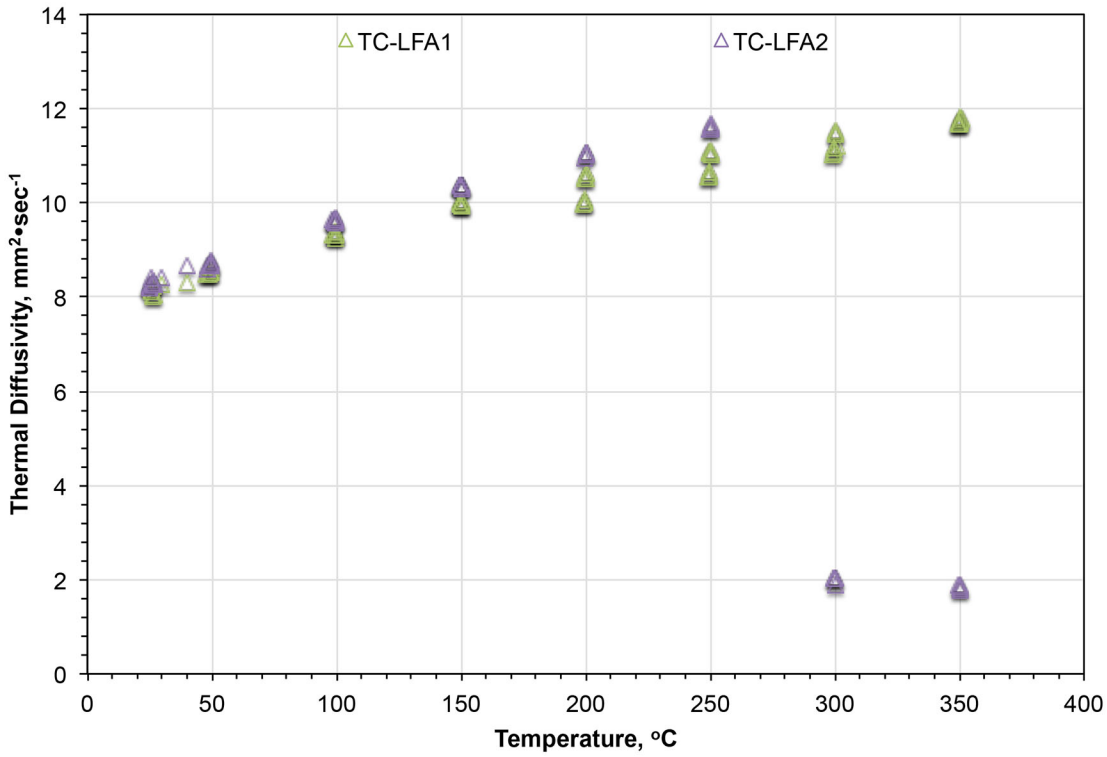

Figure 3.2. Composite Thermal Diffusivity of TC-LFA1 and TC-LFA2 Samples Obtained from LFA as a Function of Temperature

4.0 Results

Thermal diffusivity values of the TC-LFA1 and TC-LFA2 samples using the PNNL and TUM layered models are presented in this section. Thermal diffusivity was determined assuming a three-layer system (Zr + U-Mo) and a five-layer system (U-Mo).

4.1 Three-Layer System

Thermal diffusivity of the Zr + U-Mo from the TC-LFA1 and TC-LFA2 samples determined using the PNNL and TUM models is provided in Figure 4.1 as a function of temperature. In general, both models show excellent agreement for the TC-LFA1 sample. There is more discrepancy between the PNNL and TUM models for the TC-LFA2 sample, especially at temperatures above 150 °C. The PNNL model calculates slightly higher thermal diffusivity values for both samples compared to the TUM model. These differences increase at higher temperatures, i.e., at 200 °C and above. A direct comparison of the two models is shown in the scatter plot of Figure 4.2. The dashed lines on the figure represent ± 10% of the solid black line (representing a one-to-one comparison). With the exception of the measurements taken after the TC-LFA2 sample delaminated (i.e., 300 °C and greater), both models are within 10% of one another.

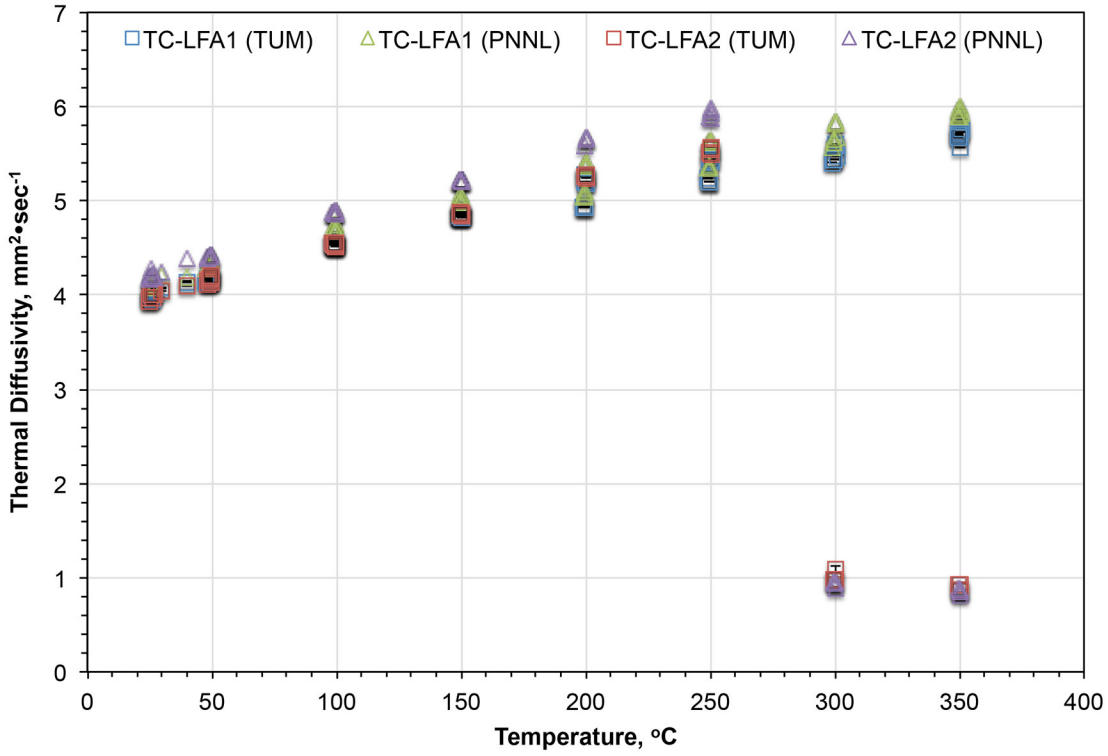

Figure 4.1. Thermal Diffusivity of the Zr + U-Mo From the TC-LFA1 and TC-LFA2 Samples as a Function of Temperature Determined Using the PNNL and TUM Models

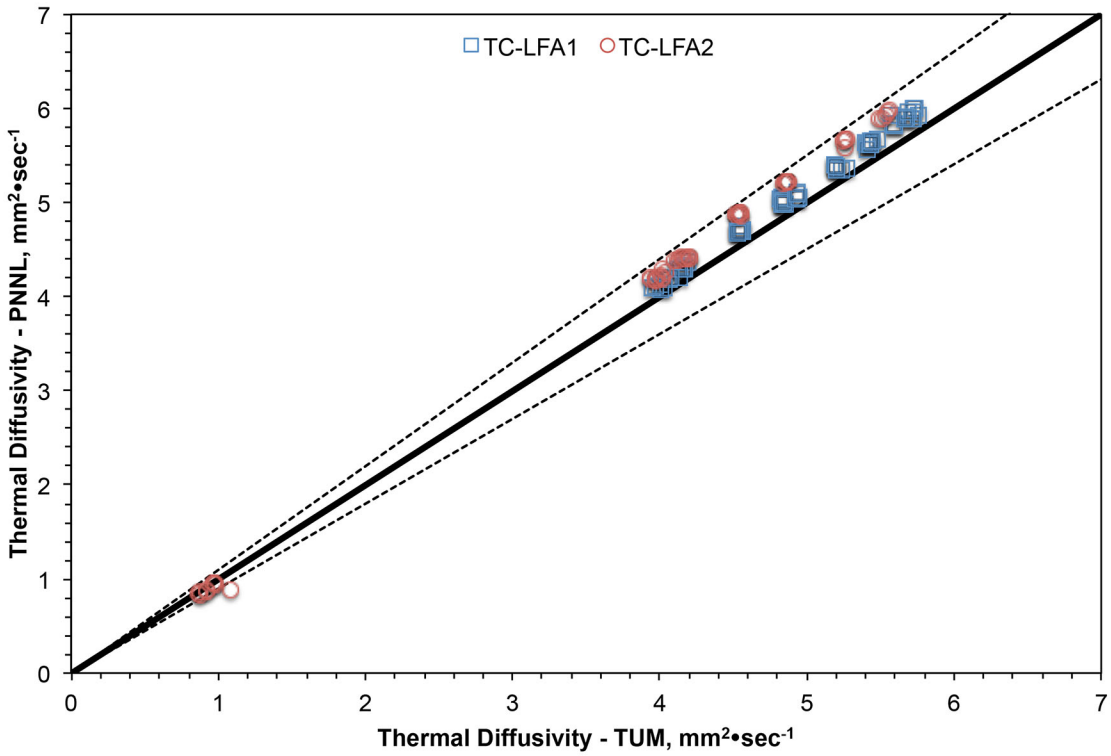

Figure 4.2. Scatter Plot of the Calculated Zr + U-Mo Thermal Diffusivity of TC-LFA1 and TC-LFA2 Using the PNNL and TUM Models

4.2 Five-Layer System

Thermal diffusivity of the U-Mo from the TC-LFA1 and TC-LFA2 samples determined using the PNNL and TUM models is provided in Figure 4.3 as a function of temperature. Similar to the three-layer results, both models generally show good agreement for the TC-LFA1 sample. The models show relatively increased disagreement for the TC-LFA2 sample, especially at temperatures above 150 ^{o}C. Again, the PNNL model calculates higher thermal diffusivity values for both samples compared to the TUM model, except at temperatures above 300 ^{o}C for the TC-LFA2 sample (after delamination occurred), where the PNNL model calculates slightly lower thermal diffusivity values. A direct comparison of the two models is shown in the scatter plot of Figure 4.4. The dashed lines on the figure represent ± 10% of the solid black line (representing a one-to-one comparison). Both five-layer models are within 10% of one another for the TC-LFA1 sample and within 15% of one another for the TC-LFA2 sample.

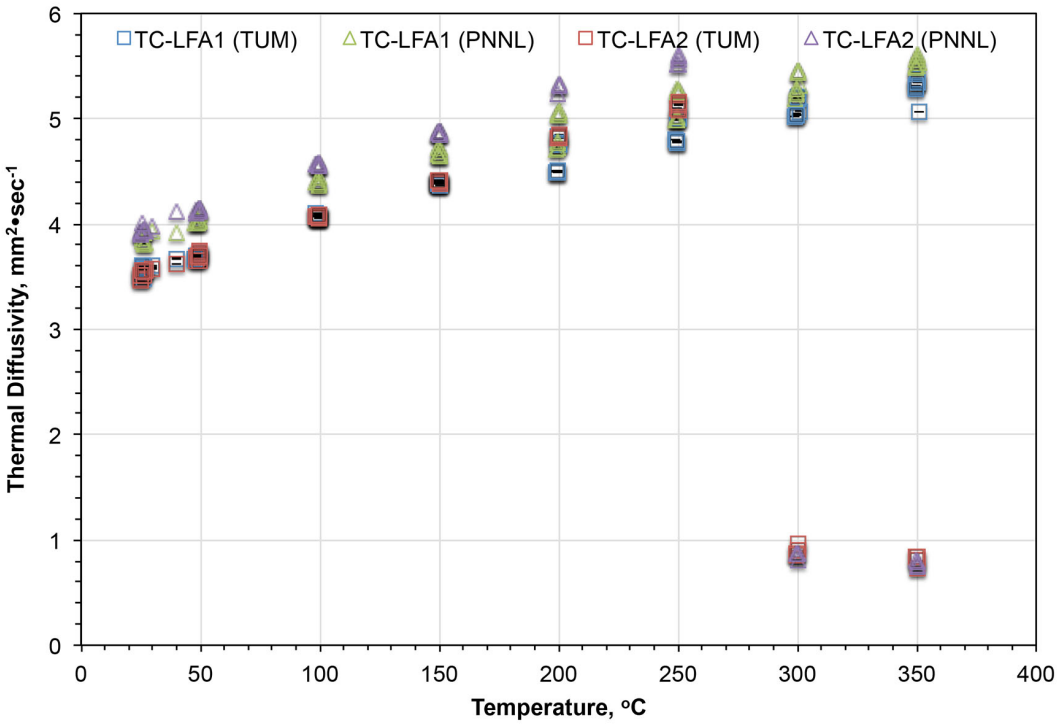

Figure 4.3. Thermal Diffusivity of the U-Mo from the TC-LFA1 and TC-LFA2 Samples as a Function of Temperature Determined Using the PNNL and TUM Models

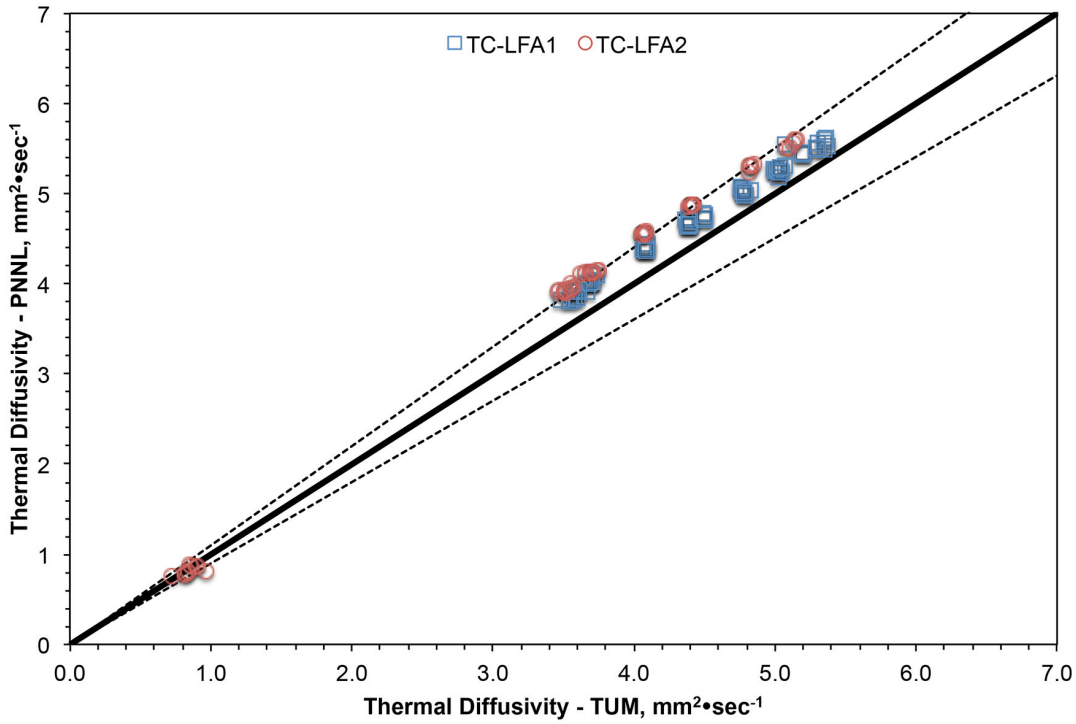

Figure 4.4. Scatter Plot of the Calculated U-Mo Thermal Diffusivity of TC-LFA1 and TC-LFA2 Using the PNNL and TUM Models

5.0 Discussion

Both numerical models yield results that are in acceptable agreement with one another, certainly within ± 15% of one another. Given the uncertainty with performing measurements on irradiated fuels of this structure, either model can therefore be used to determine the fuel thermal diffusivity from a measurement made on a multi-layered sample. Because these are the first thermal diffusivity measurements made on irradiated U-Mo alloys, it is not possible to further validate each of the models. However, the PNNL model was verified against the measurements made by Lee (Lee 1975) and validated against measurements made on unirradiated U-Mo alloy samples (Burkes et al. 2014). The TUM model was validated for one-layer systems against the standard Netzsch LFA software, as well as for multi-layer systems against CFX simulated thermal diffusivity values for LFA measurements on multi-layered plates. It can further be validated against the results determined using the PNNL model for the irradiated measurements reported here. It is important to note that besides the simplicity and initial assumptions for both models, each represents the best approach currently available in literature regarding the thermal diffusivity determination of multi-layered systems, especially irradiated nuclear fuels.

The slight variation in the results of the two models is explained by the fundamental differences in the approach and implementation of each model. The LFA instrument generates a voltage-time curve, where voltage is typically interpreted as "temperature" at time *t* on the surface opposite of where the laser energy is deposited. The PNNL model uses an input composite thermal diffusivity determined from the resultant signal processed by the Cape-Lehman plus pulse correction algorithm. This algorithm was selected because it was recommended by the instrument manufacturer as the standard fitting algorithm currently used in the field. However, calculation of the thermal diffusivity in this manner leads to slight differences between the theoretical shape of the signal and the measured signal. These differences could be the effect of contact resistance between the multiple layers and/or sapphire disk that the sample is placed upon, although no effort was made to improve the match between the theoretical and measured signals. Once the composite thermal diffusivity has been calculated, the PNNL model is used to determine the thermal diffusivity of the unknown "fuel" layer. The process assumes perfect adiabatic 1D transfer with no contact resistance. This process is fundamentally different from the TUM model, which analyzes all of these features at once, i.e., the 1D diffusion equation is discretized with zones defined based on the thickness of the sample layers. If the spatial coordinates at which the discretized model are solved in the cladding, the thermal transport properties of the cladding (e.g., conductivity, diffusivity, density, and specific heat capacity) are input into the equation and solved. If the spatial coordinates are in the "fuel" where the thermal diffusivity is unknown, it leaves this variable without a set value. The TUM model then iterates on the thermal diffusivity value of the unknown layer until the difference between the experimental signal and the signal generated by the model is minimized for all time. This likely explains the deviation of the PNNL and TUM models at temperatures at 200 ^{o}C and above, and agreement between the two models following delamination of the TC-LFA2 sample at 300 ^{o}C where contact resistance would no longer be expected to play a significant role.

The three-layer model results are generally in good agreement, but the five-layer model results yielded relatively more disagreement with one another. Again, there are some fundamental differences in the application of both models that likely contribute to these disagreements. First, the PNNL model differs from the TUM model based on the composite diffusivity input into the model. The PNNL model accepts this input determined from the built-in NETZSCH Cape-Lehman plus pulse correction algorithm, which is not as accurate as the fit the TUM model employs. Second, as the PNNL model iterates through

the three-layer and five-layer cases, the differences in composite diffusivity determination are exacerbated and increase based on errors associated with the individual layer properties, specifically in the five-layer case for Zr. Table 3.1 shows that errors associated with the relatively thin Zr layers are significantly greater than those for the AA6061 and U-Mo layers. These errors will certainly manifest them in the PNNL model approach, because they are direct inputs, and less so in the TUM model that iterates directly upon the instrument output signal. In addition, the PNNL model assumes a shape of the laser pulse delivered to the sample, while the TUM model takes the shape of the laser pulse into direct consideration. Both of these differences could be addressed in additional iterations of the PNNL model, but the benefit versus the cost must be analyzed before pursuing an endeavor, because the results are already in relatively good agreement.

The increased difference between the two models for the TC-LFA2 sample is less clear at this time. The TC-LFA1 and TC-LFA2 samples showed similar low temperature thermal diffusivity to one another, but obviously the TC-LFA2 sample delaminated at 300 ^{o}C. The "known" thermal properties (i.e., layer thickness, density, and specific heat capacity) were averaged for both samples, in the interest of simplicity. It is possible that there were slight differences in thermal properties between the two samples that could have resulted in the increased differences between TC-LFA1 and TC-LFA2 model results. Perhaps the fact that the TUM model is able to directly analyze the resultant laser flash measurement signal takes such differences into account, while the PNNL model is completely dependent upon input parameters. Again, additional analysis is needed to further investigate this problem but may not be worth the additional 5% gain in accuracy provided the ultimate uncertainty in thermal conductivity calculations on irradiated nuclear fuel.

A scatter plot comparison of the three-layer results and five-layer results is provided in Figure 5.1 for both models. The figure again reveals minor differences between the PNNL and TUM models when plotted in this manner. Excluding delamination of the TC-LFA2 sample, the three-layer model results are consistently 7-14% higher than results obtained using both five-layer models. This difference indicates the influence that the Zr diffusion layer has on the overall thermal diffusivity of the fuel plate. Irradiation damage may reduce the Zr thermal diffusivity, but is likely still higher than that of the U-Mo. However, the uncertainty associated with as-irradiated Zr thermal diffusivity may offer additional explanation on why the PNNL and TUM models diverge more for the five-layer system compared to the three-layer system. Due to the uniqueness of these measurements, it is not possible to state which approach (three-layer or five-layer) is better and/or more accurate, but due to the higher thermal diffusivity of Zr compared to U-Mo, it seems appropriate to use a five-layer model. In effect, use of the five-layer model will provide conservative thermal diffusivity values for use in fuel performance thermal conductivity and temperature calculations. Further, these results validate that the PNNL approach of using a three-layer model twice, once for "fuel" consisting of Zr and U-Mo and a second time assuming no cladding and using properties of Zr and U-Mo separately, is reasonable to extract thermal diffusivity of a composite containing five layers, although admittedly improvements to the methodology and approach could still be made.

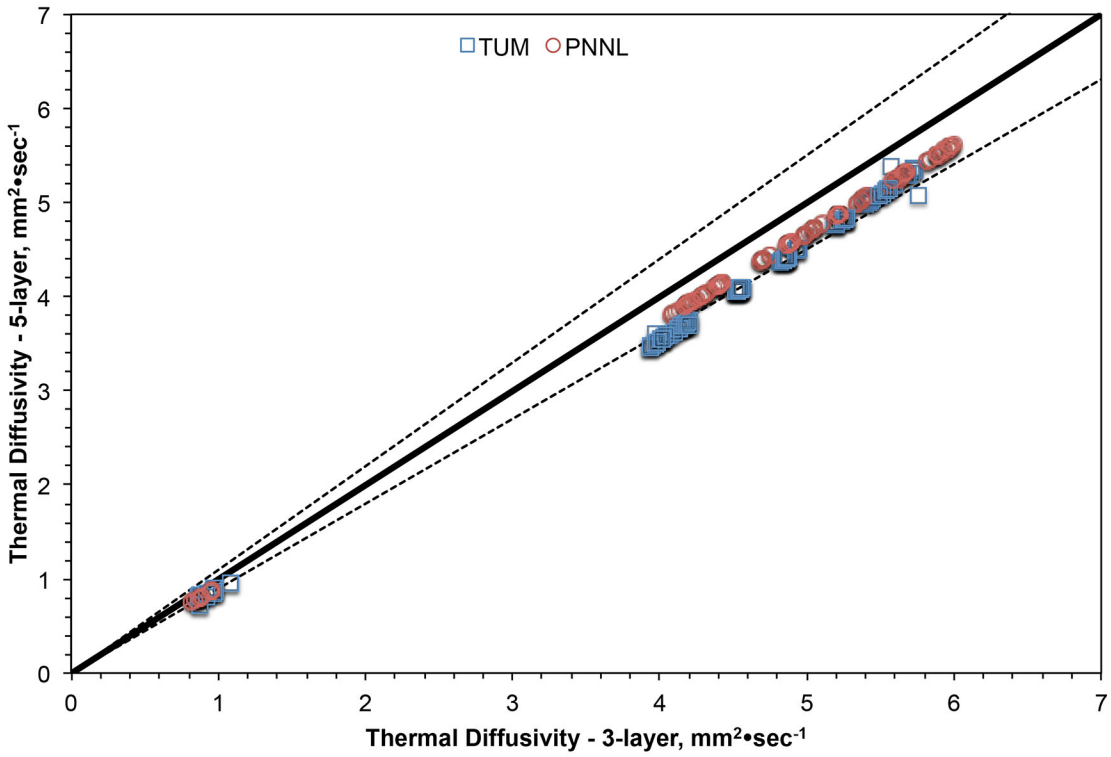

Figure 5.1. Scatter Plot Comparison of Thermal Diffusivity Obtained Using the Three-Layer and Five-Layer PNNL and TUM Models

6.0 Conclusions

A key portion of the scope associated with this project was to measure the thermal properties of fuel segments harvested from plates that were irradiated in the Advanced Test Reactor in support of the Office of Material Management and Minimization Reactor Conversion Fuel Development Pillar that is managed by Idaho National Laboratory. Thermal diffusivity of samples prepared from the fuel segments was measured using laser flash analysis. Two models, one developed by PNNL and the other developed by TUM, were evaluated to extract the thermal diffusivity of the uranium-molybdenum alloy from measurements made on the irradiated, layered composites. The two models differ in the approach and implementation of the 1D heat transport equation. The experimental data of the "TC" irradiated fuel segment was evaluated using both models considering a three-layer and five-layer system. Both models are in acceptable agreement with one another (approximately ±10%), and the minor deviations observed are attributed to the differences in approach and implementation. Both models show acceptable agreement at temperatures up to 200 ^{o}C but begin to increase in deviation from one another at temperatures of 250 ^{o}C and above. In general, use of a five-layer model results in thermal diffusivity values 7-14% lower than those obtained using a three-layer model, indicating that the influence of the zirconium diffusion barrier on the overall thermal diffusivity of the monolithic U-Mo fuel. As demonstrated in this report, either model can be used to extract fuel meat thermal diffusivity values from composite laser flash analysis measurements, and the five-layer model is recommended to more accurately represent the thermal diffusivity of the U-Mo fuel.

7.0 References

Burkes DE, AM Casella, EC Buck, AJ Casella, MK Edwards, PJ MacFarlan, KN Pool, BD Slonecker, FN Smith, FH Steen, and RE Thornhill. 2013. *Fuel Thermo-physical Characterization Project: Fiscal Year 2013 Final Report*. PNNL-22981. Pacific Northwest National Laboratory, Richland, Washington.

Burkes, DE, AM Casella, EC Buck, AJ Casella, MK Edwards, PJ MacFarlan, KN Pool, FN Smith, and FH Steen. 2014. "Development and Validation of Capabilities to Measure Thermal Properties of Layered Monolithic U-Mo Alloy Plate-type Nuclear Fuel," *Int. J. Thermophysics* 35 (8): pp. 1476-1500.

Cape JA and GW Lehman. 1963. "Temperature and Finite Pulse-Time Effects in the Flash Method for Measuring Thermal Diffusivity," *J. Appl. Phys.* 34: 1909-13.

DOD – U.S. Department of Defense. 1998. *Metallic Materials and Elements for Aerospace Vehicle Structures*. MIL-HDBK-5H, U.S. Department of Defense, Washington, D.C.

Fink JK and L Leibowitz. 1995. "Thermal Conductivity of Zirconium," *Journal of Nuclear Materials,* 226(1-2):44-50.

Lee HJ. 1975. *Thermal Diffusivity in Layered and Dispersed Composites*. Ph.D. Thesis, Purdue University, West Lafayette, Indiana.

Marquardt DW. 1963. "An Algorithm for Least-squares Estimation of Nonlinear Parameters," *SIAM* 11: 431-441.

Mills KC. 2002. *Recommended Values of Thermophysical Properties for Selected Commercial Alloys*. Woodhead Publishing Limited, Cambridge, England.

Parker WJ, RJ Jenkins, CP Butler, and GL Abbott. 1961. "Flash Method of Determining Thermal Diffusivity, Heat Capacity, and Thermal Conductivity," *J. Appl. Phys.* 32(9): 1679-84.

Distribution

No. of Copies

1 U.S. Department of Energy
National Nuclear Security Administration
Global Threat Reduction Initiative
1000 Independence Avenue
Washington, D.C. 20002
Mr. Christopher Landers
Mr. Bryan Reed (PDF)

1 Idaho National Laboratory
P.O Box 1625
Idaho Falls, ID 83415
Mr. Kenneth Rosenberg
Mr. Jason Schulthess (PDF)
Dr. Mitchell Meyer (PDF)
Dr. Barry Rabin (PDF)

1 Argonne National Laboratory
9700 S. Cass Avenue
Argonne, IL 60439
Dr. John Stevens
Dr. Erik Wilson (PDF)

1 Technische Universität München
Lichtenbergstrasse 1
D-85748 Garching
Germany
Prof. Dr. Winfried Petry
Ms. Tanja Huber (PDF)
Dr. Harald Breitkreutz (PDF)

No. of Copies

1 **Local Distribution**
Pacific Northwest National Laboratory

Douglas Burkes	K8-34
Amanda Casella	PDF
Andrew Casella	PDF
Levi Gardner	PDF
David Senor	PDF

Pacific Northwest
NATIONAL LABORATORY

Proudly Operated by **Battelle** *Since 1965*

U.S. DEPARTMENT OF
ENERGY

902 Battelle Boulevard
P.O. Box 999
Richland, WA 99352
1-888-375-PNNL (7665)
www.pnnl.gov